A 3D ELASTIC HYBRID MODELING SCHEME

RUNE MITTET[1] and BØRGE ARNTSEN[2]

[1] *Sting Research, Rosenborg gt. 17, N-7014 Trondheim, Norway.*
[2] *Statoil Research Centre, Postuttak, N-7005 Trondheim, Norway.*

(Received October 29, 1999; revised version accepted March 10, 2000)

ABSTRACT

Mittet, R. and Arntsen, B., 2000. A 3D elastic hybrid modeling scheme. *Journal of Seismic Exploration*, 9: 117-141.

Full scale 3D elastic finite-difference modeling requires very large CPU times. A hybrid modeling scheme which combines an elastic cylinder symmetric finite-difference modeling scheme with a 3D elastic finite-difference modeling schemes can reduce the CPU time considerably. The main limitation is that the overburden must be close to a plane-layer geology. The coupling of the two schemes is performed using an elastic representation theorem. Calibration of the hybrid scheme by comparison with the solution from a frequency wavenumber algorithm give good results. The fit between full 3D modeling results and hybrid modeling results for more complicated models is also acceptable.

KEY WORDS: hybrid modeling, 3-D modeling, finite-difference modeling, elastic wave propagation, complex geometry, synthetic 3D data.

INTRODUCTION

A modeling scheme giving realistic synthetic seismic data have several areas of application. One such area is verification of interpretation. If a model of the medium is constructed based on seismic and other data, then there should be some similarity between synthetic seismic data and measured seismic data, given that the modeling algorithm is sufficiently accurate. If this similarity is not

there, then either the interpreted model is not sufficiently close to the true model or the modeling scheme is not sufficiently advanced. Synthetic seismic data may also be used for survey planning. If the geometry of the main reflectors are known, then an optimal experimental configuration in terms of shot and receiver positions may be determined from modeling studies. In addition, the performance of processing software may be evaluated using synthetic data, since the processed result can be matched against the true model.

If the model to be investigated has a typical 2D geometry, then 2D finite-difference simulations may give sufficiently realistic synthetic data. All important wave modes are included but the geometrical spreading is not correct. A general absorption mechanism can be included in a 2D modeling scheme, but to allow for general anisotropic properties a 3D modeling scheme must be used. If a realistic response from a model which has a typically 3D geometry is required, then some type of 3D modeling scheme must be used. All wave modes and conversions should be included. Explicit finite-difference schemes may include all these effects. The problem, however, is that such schemes are computationally expensive. The scaling of the 3D modeling problem is typically d^4, which means that if the number of grid nodes are increased with a factor d in the three spatial dimensions, then the number of time steps must be increased with a comparable factor in order to include the relevant response. As an example, let N_X, N_Y and N_Z be the number of nodes in the three spatial directions and N_T the number of time steps. If optimized derivative operators with halflength L (Holberg, 1987) are used, then the number of numerical operations needed to calculate the response of a single shot in the purely elastic case is,

$$N_{op} = N_X N_Y N_Z N_T [18(3L-1) + 52] \quad . \tag{1}$$

A typical model may be 3500 m in the three spatial directions with a steplength of 10 m. As a minimum, 3 s of data should be generated, and a typical time step may be 0.001 s. Choosing an operator halflength of 6 implies that the calculation can be performed at 2.6 grid points per shortest wavelength. For the purely elastic problem, neglecting absorption and anisotropy, the CPU time at 1 Gflops is 13 hours. This may be acceptable for experiments with a few shots, but not for simulation of a marine survey with several hundreds of shots or more. To resolve this problem with the indicated computer resources and without inventing a completely new modeling method some approximation must be performed.

The solution is in this work limited to typically North-Sea problems where there is a plane-layered overburden over a structurally more complicated target

If a plane-layered overburden is assumed, then a cylindrical-symmetric scheme can be used here to calculate the Greens tensor. This scheme obeys 3D elastic wave propagation. Normally, a cylindrical-symmetric scheme gives the solution as a function of radial coordinate r and depth coordinate z, but the symmetries of the elastic field can be used to find the solution on a horizontal surface at a desired depth in the model. The symmetries of the field can also be used to convert the cylindrical-symmetric Greens tensor to a Cartesian Greens tensor. The elastic field on this coupling surface serves as a boundary condition for the modeling scheme used in the deeper part of the model. In the deeper part of the model a full scale 3D elastic finite-difference scheme is used.

This hybrid method reduces the size of the full 3D modeling problem in three ways. Firstly, the actual size of the 3D grid is reduced since the 3D elastic finite-difference scheme is used in the deeper part of the model only. Secondly, the spatial sampling intervals may be increased since the S-wave velocities generally are higher at larger depths. Increased spatial sampling intervals implies less nodes and hence a reduced number of numerical operations. Thirdly, the 3D elastic finite-difference scheme can be solved for a reduced number of timesteps. The initial time of the 3D simulation is given by the time the field requires to reach the depth where the 3D elastic finite-difference scheme is used and the final time is given by the desired time for the shot record minus the time required to propagate the solution from the depth where the 3D elastic finite-difference scheme is used up to the receivers. The CPU time required to perform the cylinder-symmetric modeling in the overburden is negligible compared to the CPU time of the full 3D elastic finite-difference scheme. The reduction factor in CPU time using the hybrid scheme as compared to the full 3D elastic scheme is model dependent, but is typically of order 10 (5-15) for a full size model, however for models with high velocity contrasts from top to bottom and a deep target volume the reduction factor may be of order 100.

It is nothing in the formalism presented here that prevents the cylinder-symmetric finite-difference scheme from being substituted with a 3D ray-tracing algorithm. This would allow for a more general geology in the overburden at the possible cost of neglecting important events in the overburden. If the overburden has no symmetries, then the Green's tensor from each node at the coupling depth to each receiver must be calculated. This may be a time consuming process.

THEORY

The basic properties of the model are shown in Fig. 1. The model consist of a plane-layer geology over a 3D generally inhomogeneous target volume. The

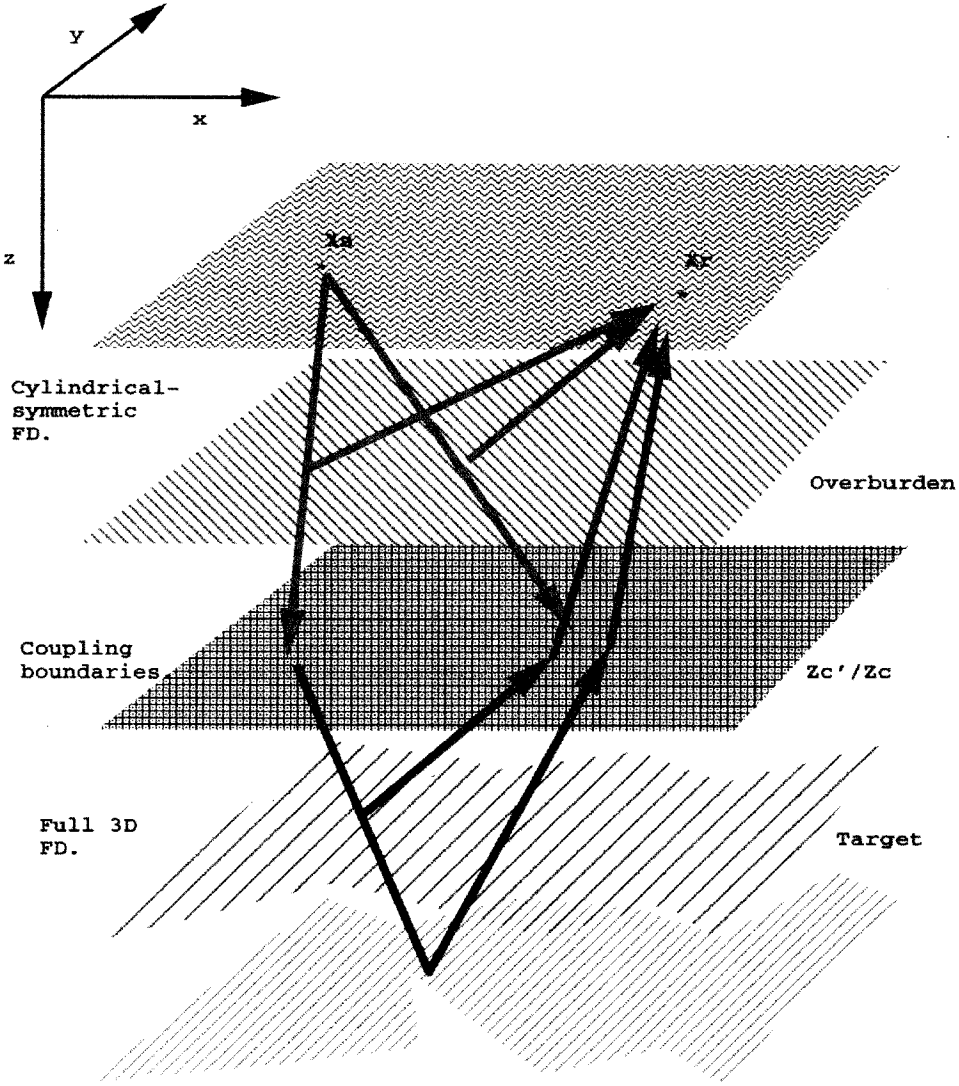

Fig. 1. The model is separated into two volumes. The green and red arrows indicate the part of the

be coupled. This coupling is formally performed at a horizontal surface with coordinate $\mathbf{x}_c$. The problems of using a single coupling surface will be discussed in a separate section. The present solution will be to split this surface into two surfaces, where the downgoing field is a boundary condition at $\mathbf{x}_c$ and the upgoing field is a boundary condition at $\mathbf{x}_c'$, where $\mathbf{x}_c'$ is slightly above $\mathbf{x}_c$. It is, in principle, possible to obtain the complete solution to the wavefield for these types of models using the indicated hybrid modeling method (dynamic coupling), but in order to reduce overall CPU time a simplified solution (static coupling) is chosen. In this simplified approach, all direct events and conversions plus the internal multiples in the overburden are included in the shotgather. The direct events and conversions plus internal multiples in the target volume are also included, but internal multiples interacting both with the overburden and the target volume are neglected. These events could have been included using the dynamic coupling approach. In the dynamic coupling approach the cylinder-symmetric and full 3D scheme must run simultaneously with coupling of the fields for each timestep. In the static approach the cylinder-symmetric modeling can be performed before running the full 3D scheme.

Let the source be located at $\mathbf{x}_s$ and the receivers at $\mathbf{x}_r$. Three finite-difference simulations are needed to generate the desired response. An elastic cylindrical-symmetric finite-difference calculation can generate the response at $\mathbf{x}_r$ due to reflections in the overburden. The same calculation can generate a downgoing field at the coupling depth $\mathbf{x}_c$. This downgoing field serves as a boundary condition for a full 3D finite-difference calculation giving the response from the target volume. The resulting upgoing field from this simulation is recorded at $\mathbf{x}_c'$ and serves as a new boundary condition. A second cylindrical-symmetric finite-difference simulation is performed in order to obtain the Green's tensor which can propagate the field from $\mathbf{x}_c'$ to $\mathbf{x}_r$.

In the present version of the hybrid scheme a marine experimental configuration is assumed. Thus, the source is located in the water layer and hydrophone measurements are performed. It is further assumed that the elastic part of the model is isotropic.

The elastic Green's tensor G_{ijnm} is given by the equation

$$\partial_t^2 G_{ijmn}(\mathbf{x},t\,|\,\mathbf{x}',t') - c_{ijpq}(\mathbf{x})[\partial_p \rho^{-1}(\mathbf{x})\partial_k G_{qkmn}(\mathbf{x},t\,|\,\mathbf{x}',t')]$$

$$= c_{ijmn}(\mathbf{x})\delta(\mathbf{x} - \mathbf{x}')\delta(t - t') \quad , \tag{2}$$

where the elastic Hooke's tensor reduces to

in the isotropic case. Here λ and μ are the Lamé parameters and ρ is the density.

With the Green's tensor from equation (2), the stress tensor is given as in Mittet et al. (1994),

$$\begin{aligned}\sigma_{mn}(\mathbf{x},t) = &\int_0^{t^+} dt' \int d^3x' G_{mnij}(\mathbf{x},t-t'|\mathbf{x}',0)\partial_i'\rho^{-1}(\mathbf{x}')f_j(\mathbf{x}',t) \\ &+ \int_0^{t^+} dt' \oint_S dS(\mathbf{x}')\{G_{mnij}(\mathbf{x},t-t'|\mathbf{x}',0)n_i a_j(\mathbf{x}',t') \\ &- [\partial_i' G_{mnij}(\mathbf{x},t-t'|\mathbf{x}',0)]t_j(\mathbf{x}',t')\} \\ &+ \int d^3x'\{[\partial_{t'} G_{mnij}(\mathbf{x},t-t'|\mathbf{x}',0)]\epsilon_{ij}(\mathbf{x}',t') \\ &- G_{mnij}(\mathbf{x},t-t'|\mathbf{x}',0)\partial_{t'}\epsilon_{ij}(\mathbf{x}',t')\}|_0^{t^+} \quad . \end{aligned} \tag{4}$$

Here, σ_{mn} is a component of the stress tensor, a_i is a component of the particle acceleration vector, ϵ_{ij} is a component of the strain tensor and the reduced traction, t_j, is given by,

$$t_j(\mathbf{x}',t') = n_p\sigma_{jp}(\mathbf{x}',t')/\rho(\mathbf{x}') \quad , \tag{5}$$

where n_i is a component of the surface normal. Assuming initial and final condition to be zero, equation (4) can be separated into a contribution due to the exciting force $f_j(\mathbf{x}',t)$,

$$\sigma_{mn}^f(\mathbf{x},t) = \int_0^{t^+} dt' \int d^3x' G_{mnij}(\mathbf{x},t-t'|\mathbf{x}',0)\partial_i'\rho^{-1}(\mathbf{x}')f_j(\mathbf{x}',t) \quad , \tag{6}$$

and a boundary value contribution,

$$\begin{aligned}\sigma_{mn}^b(\mathbf{x},t) = &\int_0^{t^+} dt' \oint_S dS(\mathbf{x}')\{G_{mnij}(\mathbf{x},t-t'|\mathbf{x}',0)n_i a_j(\mathbf{x}',t') \\ &- [\partial_i' G_{mnij}(\mathbf{x},t-t'|\mathbf{x}',0)]t_j(\mathbf{x}',t')\} \quad . \end{aligned} \tag{7}$$

If the field representing the boundary condition is propagating in one direction only, then it is sufficient to know the boundary condition on a horizontal surface which in principle must have infinite aperture, the need for a closed surface integral can be relaxed.

Within the given approximation, the field due to a source at $\mathbf{x}_s$ is purely downgoing at $\mathbf{x}$ and the response from the target volume is purely upgoing at

excited by the source and modeled with the cylindrical-symmetric scheme, with the 3D finite-difference simulation and to couple the upgoing 3D finite-difference response from the target volume with the cylindrical-symmetric Greens tensor giving the pressure response at the receivers. The total pressure response at the receivers are found from a summation of the pressure given in equation (A-7) and the pressure given in equation (C-2).

BOUNDARY CONDITIONS

The boundary condition for the stress field is given in equation (7). This boundary condition, input to the 3D finite-difference scheme, is calculated with the cylindrical-symmetric finite-difference scheme and represents a downgoing field at the coupling surface at depth z_c. If the boundary condition is properly implemented at the coupling surface, then it results in a purely downgoing traction field at this depth. The total traction response at this coupling surface is this downgoing traction plus the upgoing traction resulting from reflections below z_c. In order to have a purely upgoing traction field at depth z_c, needed for extrapolation of the field at this depth up to the receivers, the downgoing traction should be subtracted from the total traction response. This is a straight forward procedure.

The boundary condition used here give a purely downgoing traction at and below z_c. This leads to a stress tensor in the 3D elastic modeling scheme which is zero above z_c. This points to a step-like behavior in depth of the stress field. The corresponding acceleration components can be obtained from the equation of motion and are proportional the z-derivatives of some of the stress field components. This gives a delta-function behavior of the acceleration field at the coupling depth z_c which is added to the downgoing and upgoing acceleration components at z_c. In order to have a purely upgoing acceleration field at depth z_c the delta-function contribution and the downgoing acceleration should be subtracted from the total acceleration response. Band-limited delta-function are difficult to treat in numerical schemes and a method which satisfactorily removed this delta-function (less than 1 percent error) independent of steplengths and frequency content was not found. The hybrid scheme can also be implemented with the boundary condition for the displacement (Aki and Richards, 1980). In this case the displacement field have a step-like behavior at depth z_c and there are delta-function contributions to the stress field which must be removed. Thus, the problem is not solved using this representation theorem as compared to the one given in equation (7).

A method which seems to work satisfactorily is to split the coupling surface at depth z_c into two. A new coupling surface at depth z_c' is introduced.

that only upgoing fields are recorded at depth z_c' and these fields serve as the boundary condition for propagating the field to the receivers using the Greens tensor calculated with the cylindrical-symmetric scheme. There is still a delta-function contribution centered at depth z_c, but this contribution is not seen at depth z_c'.

Cylindrical-symmetric finite-difference.

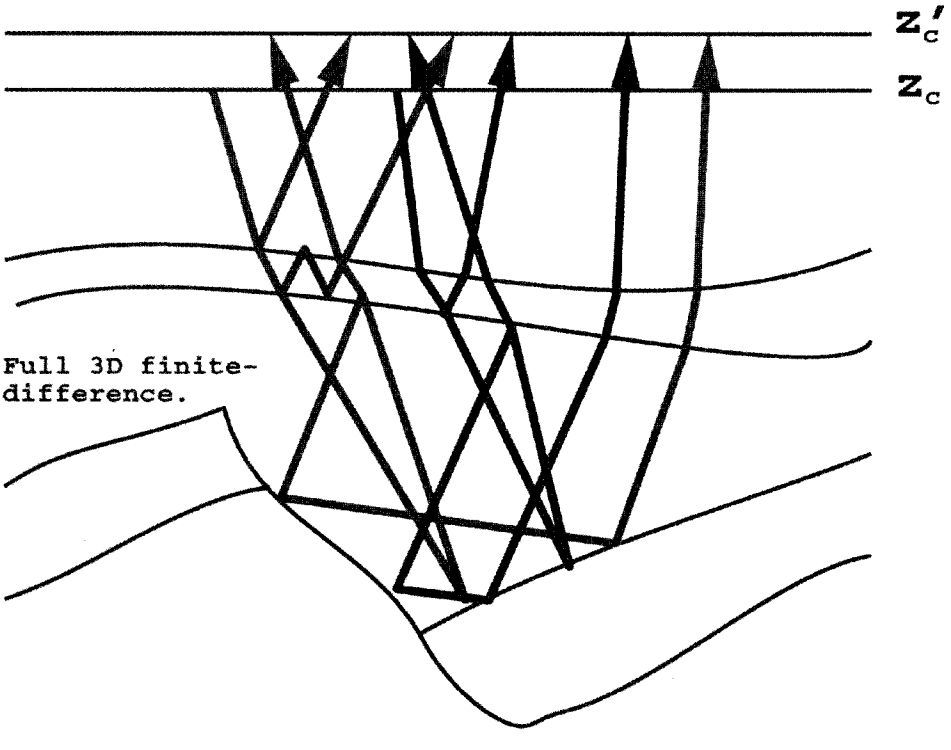

Fig. 2. Cross section of 3D model. The downgoing field is zero just below the

NUMERICAL EXAMPLES

The finite-difference modeling program used here can be started in three different modes. A pure cylindrical-symmetric calculation assuming a plane-layer earth model can be performed, a pure 3D finite-difference calculation can be performed or a hybrid calculation can be performed. In the case of a plane-layer model these three schemes should give the same response if the interaction between the overburden and the target volume is sufficiently small. The last criterion is relevant only for the hybrid scheme. A cross section of a plane-layer 3D model is shown in Fig. 3 and the parameters are specified in Table 1. This model is used for calibration of the three modeling schemes. As a reference, the response for this model is also calculated using the OSIRIS modeling package. The OSIRIS modeling package is based on a direct global matrix method (Schmidt and Jensen, 1985).

Table 1. Physical parameters of each layer for plane-layer model.

Layer	Depth [m]	ρ[kg/m^3]	V_p [m/s]	V_s [m/s]
I	195	1000	1500	0
II	495	2000	2000	1200
III	∞	2500	2500	1500

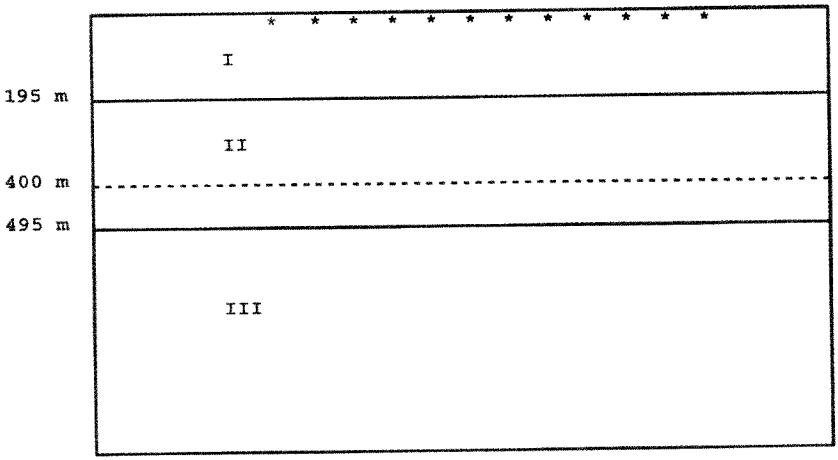

Table 2. Approximate arrival times at offset 100 m.

Event	Arrival time [s]
Direct wave	0.1
Water bottom reflection	0.30
First water bottom multiple	0.56
Second water bottom multiple	0.82
P-wave reflection from second interface	0.60
S-wave reflection from second interface	0.70
P-wave multiple in second layer	0.75

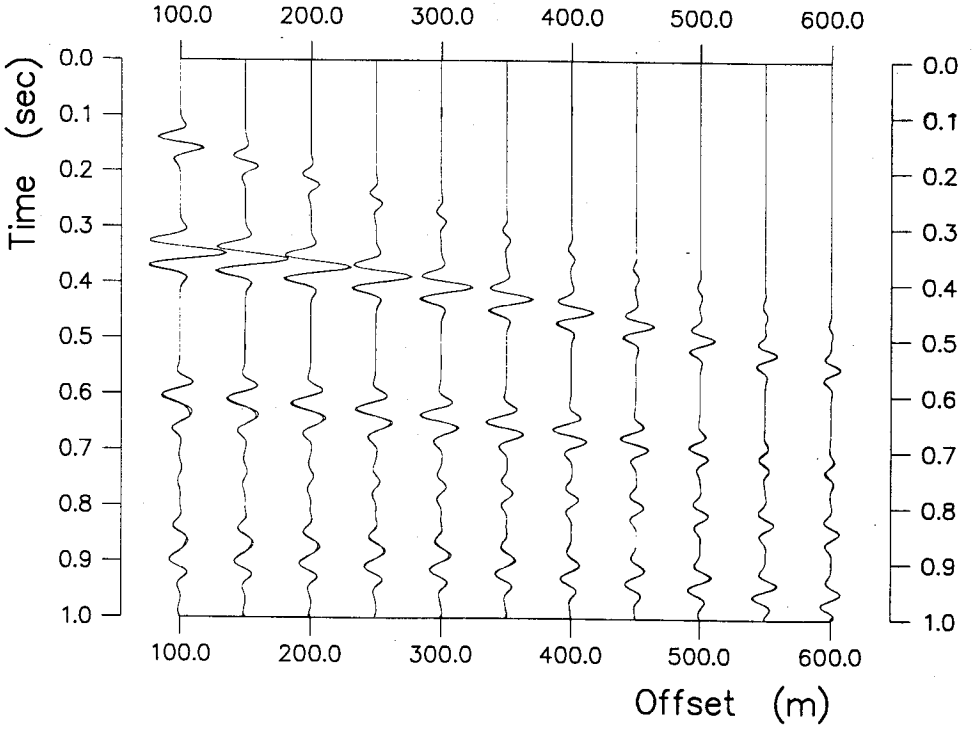

Fig. 4. OSIRIS and cylindrical-symmetric finite-difference response.

Some approximate arrival times at offset 100 m for the model shown in Fig. 3 are given in Table 2. In Fig. 4 the OSIRIS modeling response and the

with some small deviations for the combined event starting at 0.56 s at the nearest offset. This event is an interference pattern of the first water-bottom multiple and the P-P reflection at the second interface. The event starting at 0.7 s is from the downgoing P-wave reflected as an S-wave at the second interface and then converted to a P-wave at the water bottom, before reaching the hydrophones. The amplitude of this event clearly increases with increasing offset. In Fig. 5 the OSIRIS modeling response and the 3D finite-difference response are plotted. The 3D finite-difference response and the cylindrical-symmetric response are identical so there is a good fit also for these two modeling methods. The OSIRIS modeling response and the hybrid response are shown in Fig. 6. The coupling depths for the hybrid modeling are at approximately 400 m. Also here a good fit between the modeling responses is obtained. The internal multiple in layer II, expected to arrive at 0.75 s at near offsets, is not included in the hybrid modeling response. The amplitude of this event seems to be negligible since the number of events appear to be similar in the two shotgathers. The fit between the two shotgathers is somewhat poorer at high offsets, compared to the two previous examples. This may be an aperture effect since the boundary surface at depth z_c' have a limited aperture in order to minimize CPU time.

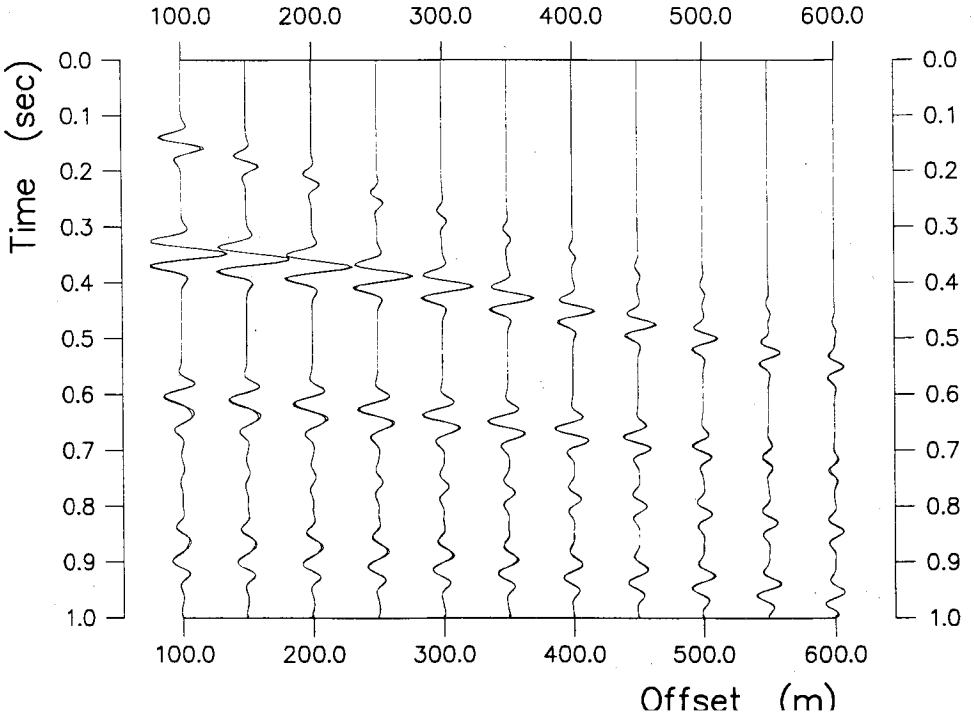

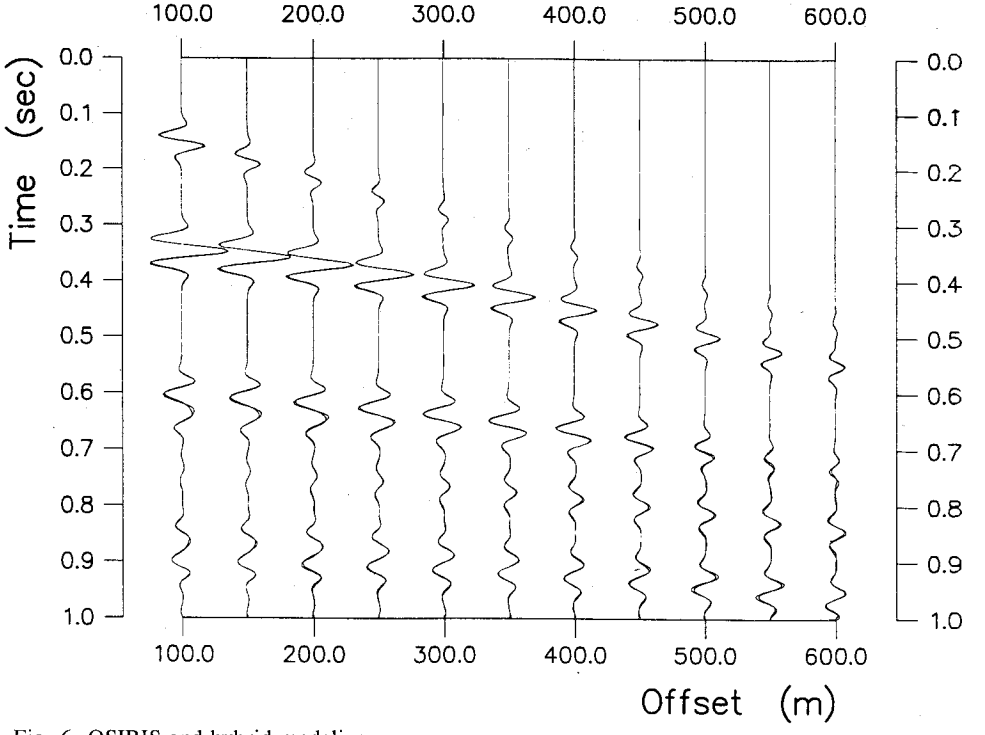

Fig. 6. OSIRIS and hybrid modeling response.

In Fig. 7 the cross section of a faulted 3D model is shown. The parameters are as for the previous model, but the second interface has here a step behavior. The response for this model can be calculated correctly with the full 3D modeling scheme only. The hybrid modeling scheme may give good approximate solution, whereas the OSIRIS and the pure cylindrical-symmetric finite-difference schemes can give plane-layer responses only. The result of comparing the 3D finite-difference response for the second model with the OSIRIS response for the first model is shown in Fig. 8. As expected, the two shotgathers are different at small offsets where the two models are different and similar at higher offsets where the two models are identical. In Fig. 9 the 3D finite-difference response for the faulted model is plotted with the cylindrical-symmetric finite-difference response for a plane-layer model with the second interface at depth 595 m. The differences are here small at small offsets where the models are identical and the differences are larger at higher offsets where the models are different. The 3D finite-difference shotgather and the hybrid modeling shotgather for the faulted model are plotted in Fig. 10. Here the fit is fairly good at all offsets. The small differences can probably again be explained by the limited aperture of the coupling boundary at depth z_0'. The

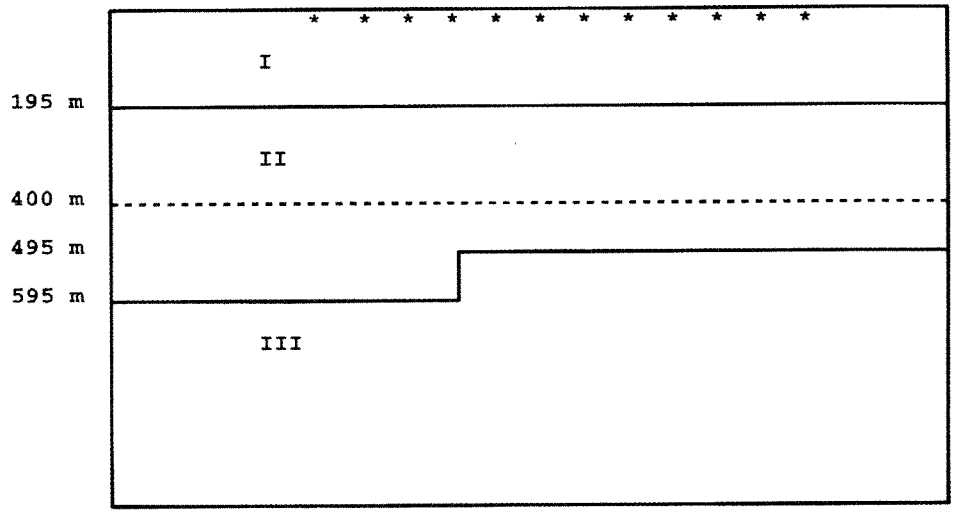

Fig. 7. Faulted model. The source is indicated with a red star. The receivers are indicated with blue stars. The coupling depths for the hybrid scheme are indicated with the dashed line.

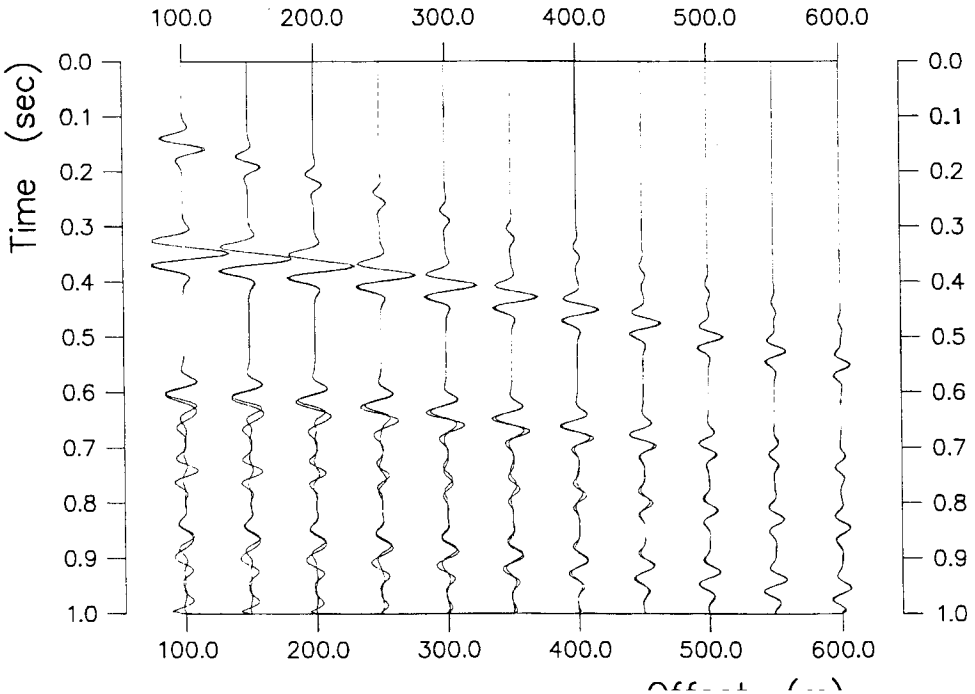

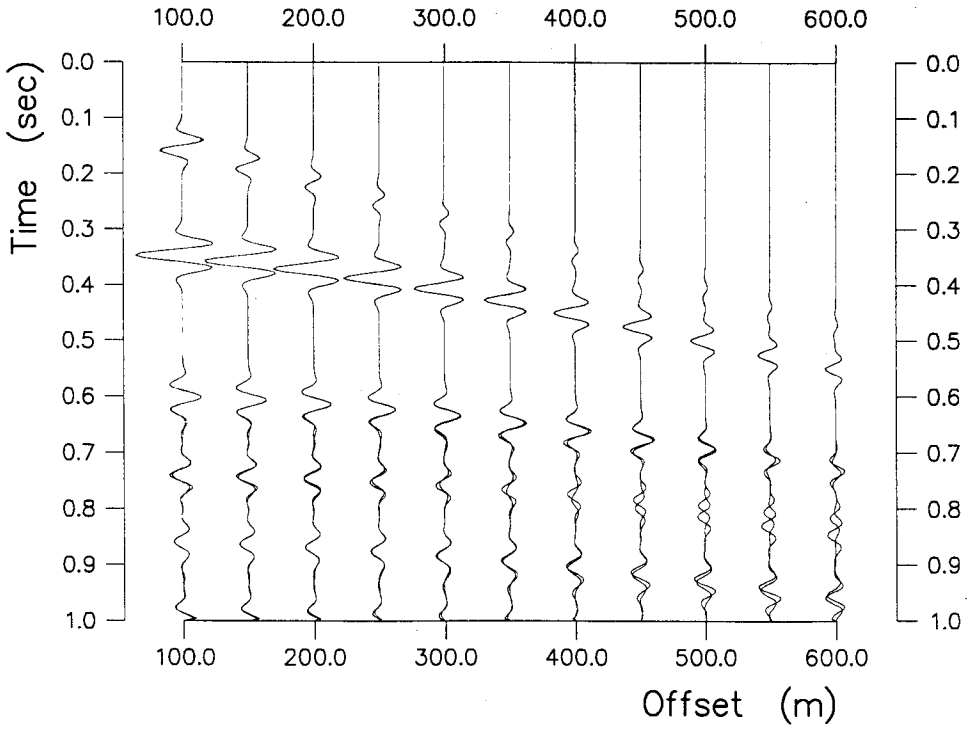

Fig. 9. 3D finite-difference and cylindrical-symmetric response.

The scheme is also tested for a larger model with a 3D geometry. The model is shown in Fig. 11. The model has a surface area which is 4 km by 4 km and it is 3 km in depth. The model is built from three subvolumes each having a similar fault structure in the inline (x-) direction. The fault structure is deepest for the central part of the model. The source is located at x=900 m, y=2000 m with a depth of 10 m. The receivers have offsets from 1000 m to 3000 m with y=2000 m and depth 10 m. Thus, the experiment is performed over the central block and noticeable side-scatter effects should appear.

Three modeling runs were performed. First a full 3D elastic modeling was performed in order to obtain a reference shotgather. Then a cylinder-symmetric modeling was performed. The density and velocity models as functions of depth were taken from the 3D model at x-position 950 m and y position 2000 m. This is midway between the source and the nearest offset hydrophone. Finally a hybrid modeling was performed. The coupling depths for the hybrid scheme

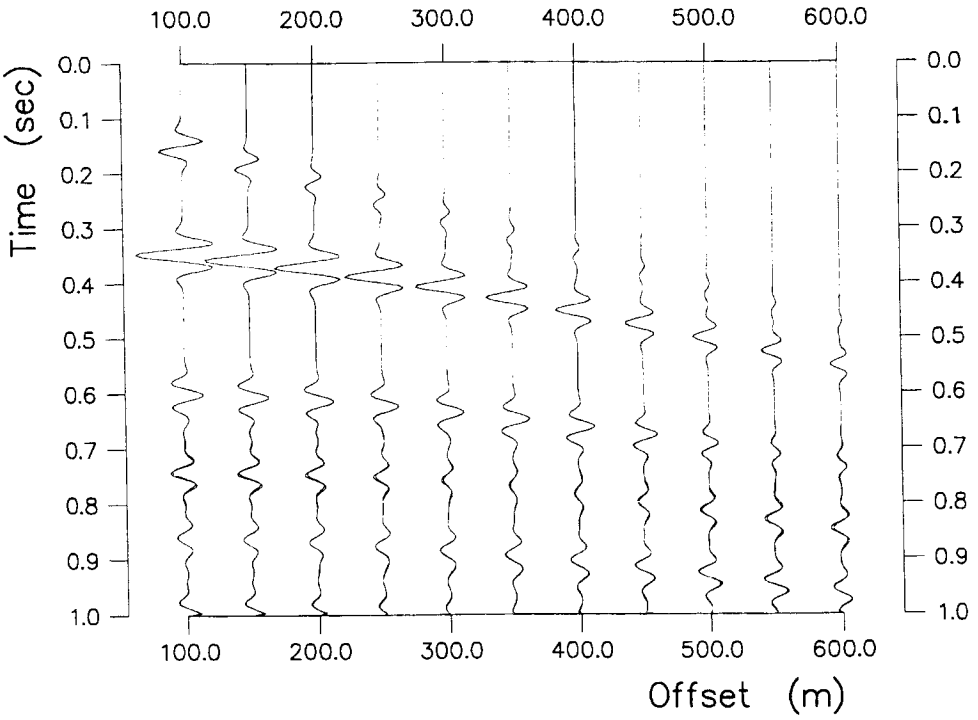

Fig. 10. 3D finite-difference and hybrid modeling response.

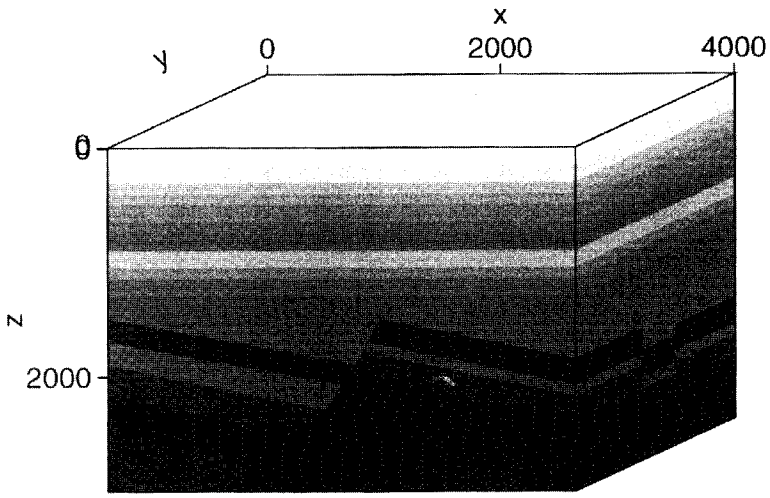

The resulting reference shotgather is shown in Fig. 12, the shotgather resulting from the cylinder-symmetric modeling is shown in Fig. 13 and the result of the hybrid modeling is shown in Fig. 14. For comparison selected traces from the reference shotgather and the shotgather resulting from the cylinder-symmetric modeling is shown in Fig. 15. As expected, the traces coincide at the earliest times when only the plane-layer response is measured. At later times the reference shotgather contain the full 3D response of the model and the two shotgathers differs significantly. For more detail the traces at offset 1600 m are shown in Fig. 16. Selected traces from the reference shotgather and the shotgather resulting from the hybrid modeling is shown in Fig. 17. There are some small differences, but the fit between the two datasets is good at all times and offsets. For more detail the traces at offset 1600 m are shown in Fig. 18. The remaining differences can probably be contributed to the limited aperture of the coupling surfaces and to the neglected multiple interactions between the overburden and the target volume. However, these modeling results indicate that the events not included in the hybrid modeling are small and that acceptable results can be obtained with the hybrid modeling scheme, even for 3D models with a complicated target volume. The modeling were run on 8 Silicon Graphics R10000 processors. For this particular example, the reduction in CPU time was a factor 11 using the hybrid modeling scheme as compared to the 3D modeling scheme.

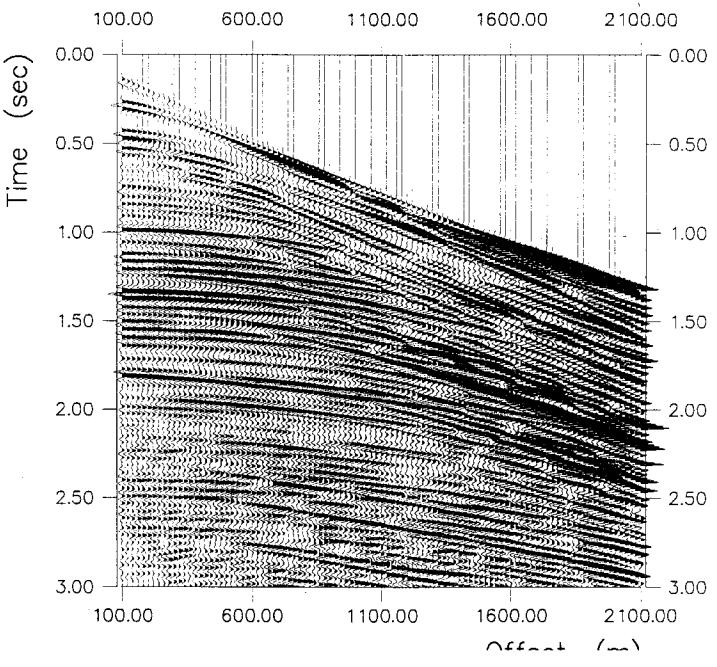

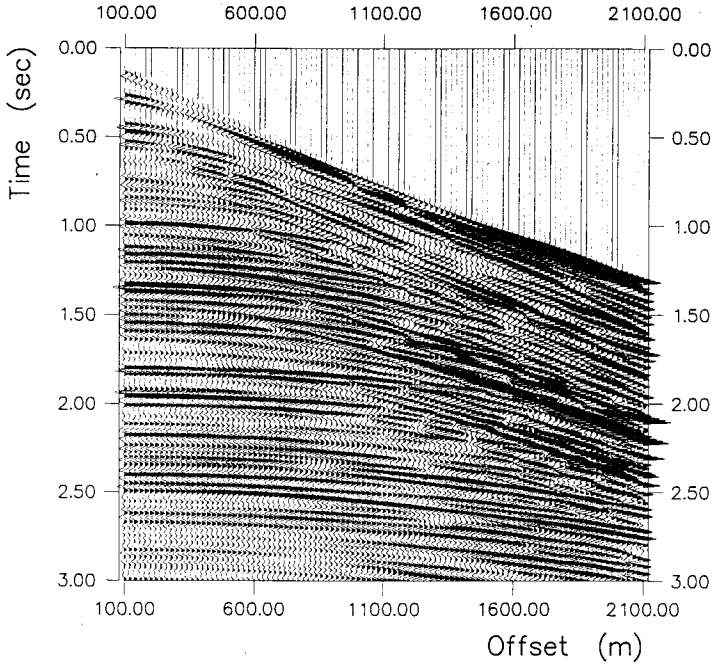

Fig. 13. Cylinder-symmetric modeling response. Traces are scaled with t^2.

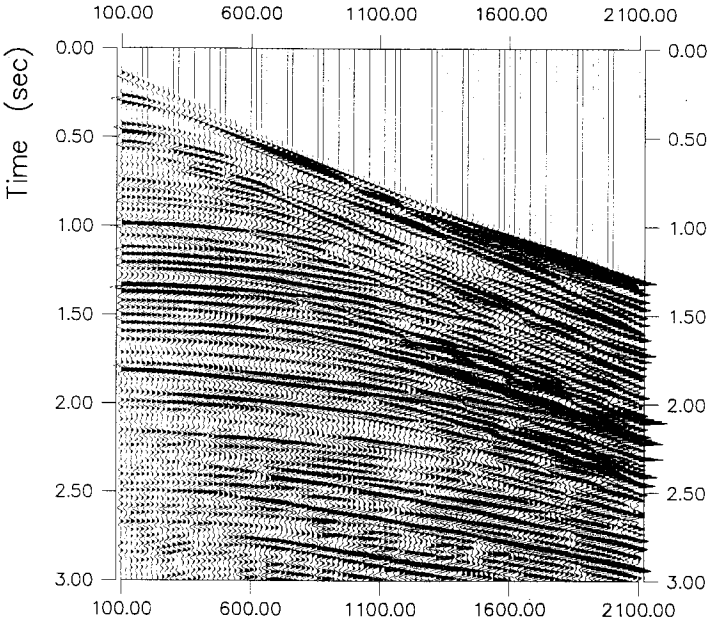

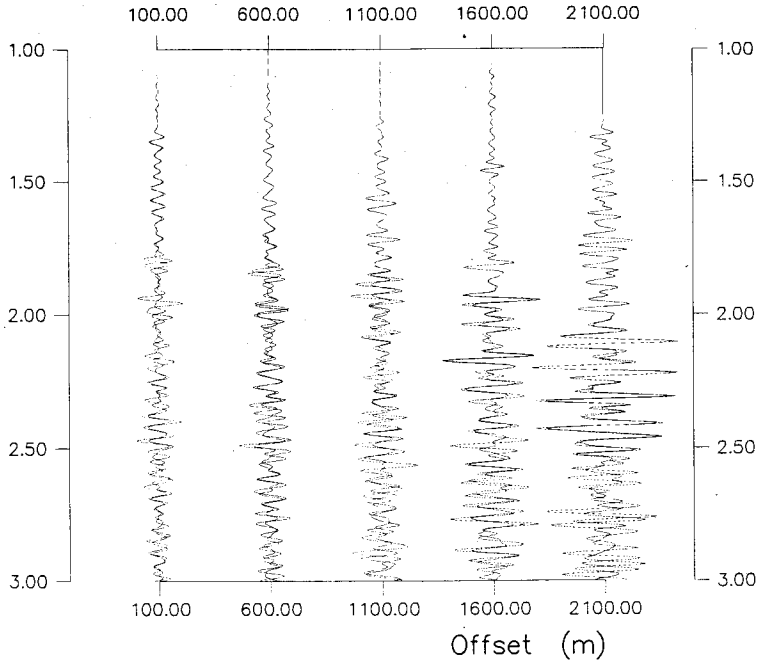

Fig. 15. Selected traces for reference data and cylinder-symmetric data. The time scale is from 1 second to 3 seconds. Traces are scaled with t^2.

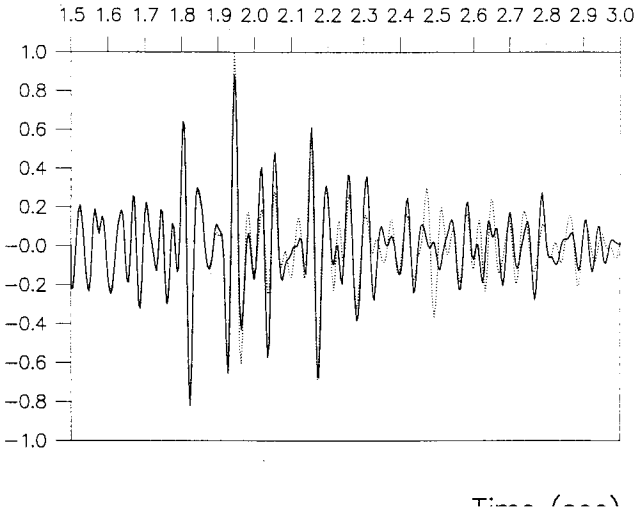

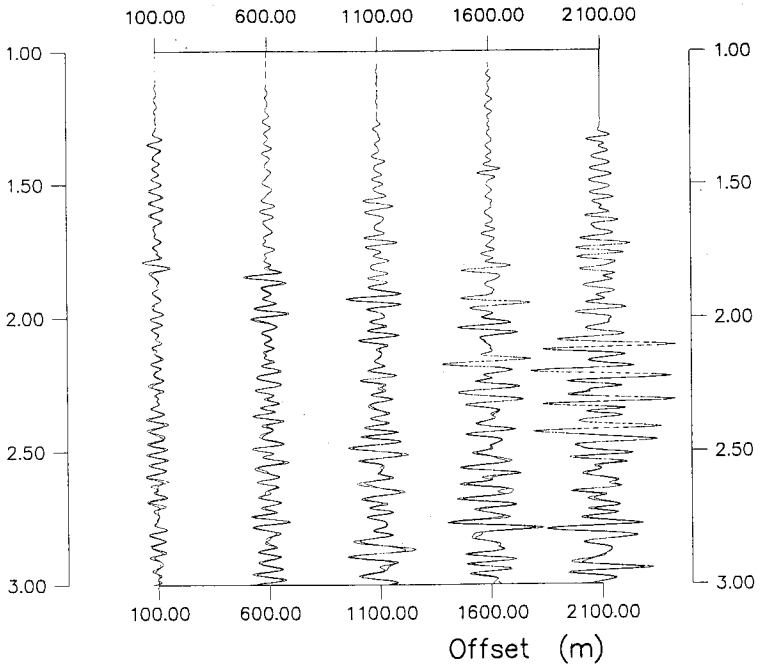

Fig. 17. Selected traces for reference data and hybrid data. The time scale is from 1 second to 3 seconds. Traces are scaled with t^2.

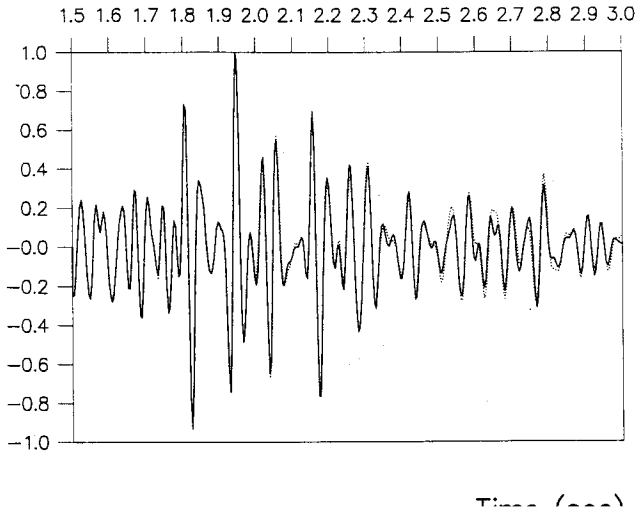

CONCLUSION

A hybrid modeling scheme combining an elastic cylinder symmetric finite-difference modeling scheme with a 3D elastic finite-difference modeling scheme has been presented. The coupling of the two methods is performed using an elastic representation theorem for the stress field.

The scheme was tested for a plane-layered model giving good agreement with a frequency-wavenumber solution. For models with more complicated 2D and 3D geometries the hybrid scheme was compared with the full 3D elastic finite-difference scheme. Also here the resulting shotgathers were in good agreement. Modeling results indicate that the events not included in the hybrid modeling are small and that acceptable results can be obtained with the hybrid modeling scheme, even for 3D models with a complicated target volume.

ACKNOWLEDGEMENTS

This work has been financially supported by Statoil Research. We thank Statoil Research for the permission to publish this paper.

REFERENCES

Aki, K. and Richards, P.G., 1980. Quantitative Seismology. W.H. Freeman and Co., San Francisco.

Holberg, O., 1987. Computational aspects of the choice of operator and sampling interval for numerical differentiation in large-scale simulation of wave phenomena. Geophys. Prosp., 37: 629-655.

Mittet, R., 1994. Implementation of the Kirchhoff integral for elastic waves in staggered-grid modeling schemes. Geophysics, 59: 1894-1901.

Mittet, R., Amundsen, L. and Arntsen, B., 1994. Iterative inversion/migration with complete boundary conditions for the residual misfit field. J. Seismic Expl., 3: 141-156.

Mittet, R., Holberg, O., Arntsen, B. and Amundsen, L., 1988. Fast finite-difference modeling of 3-D elastic wave propagation. Expanded Abstr., 58th Ann. Internat. SEG Mtg., Anaheim: 1308-1311.

Mittet, R. and Renlie, R., 1996. High-order finite-difference modeling of multipole logging in formations with anisotropic attenuation and elasticity. Geophysics, 61: 21-33.

Schmidt, H. and Jensen, F.B., 1985. Efficient numerical solution techniques for wave propagation in horizontally stratified environments. Computers and Mathem. with Applic., 11: 699-715.

APPENDIX A

Cylinder symmetric elastic finite-difference modeling of overburden response and downgoing field.

If the source is assumed to be in the water layer, then the source term is curl free and only normal components of the source tensor contributes, thus it is sufficient to calculate the Greens tensor $G_{ijmm}(\mathbf{x}_c,t|\mathbf{x}_s,t')$ in the overburden to obtain the downgoing field at $\mathbf{x}_c$. The Greens tensor is simplified due to the cylindrical symmetry,

$$G_{ijmm}(\mathbf{x}_c,t|\mathbf{x}_s,t') = G_{ijmm}(r_c-r_s,z_c,t-t'|0,z_s,0) \quad , \tag{A-1}$$

where

$$r_c = \sqrt{(x_c^2 + y_c^2)} \quad , \qquad r_s = \sqrt{(x_s^2 + y_s^2)} \quad . \tag{A-2}$$

For the cylindrical-symmetric scheme used in the overburden the spatial translation invariance is used and hence, $r_s = 0$. Thus, the Green's tensor $G_{ijmm}(r_c,z_c,t-t'|0,z_s,0)$ has to be calculated.

The set of coupled partial differential equations in cylindrical coordinates for elastic wave propagation in an absorbing and anisotropic (TI) medium are given in Mittet and Renlie (1996). The notation is simplified using $\tau = t-t'$ and thus $G_{ijmm}(r,z,t-t'|0,z_s,0) = G_{ijmm}(r,\tau,z|z_s)$. Assuming a non-absorbing and isotropic medium with a spherically symmetric source being a band-limited delta function in space and time the equations to solve become

$$\begin{aligned}
A_{rmm}(r,\tau,z|z_s) &= \rho(r,z)^{-1}[\partial_r G_{rrmm}(r,\tau,z|z_s) \\
&+ (1/r)[G_{rrmm}(r,\tau,z|z_s) - G_{\theta\theta mm}(r,\tau,z|z_s) + \partial_z G_{rzmm}(r,\tau,z|z_s)] \quad , \\
A_{zmm}(r,\tau,z|z_s) &= \rho(r,z)^{-1}[\partial_z G_{zzmm}(r,\tau,z|z_s) \\
&+ \partial_r G_{rzmm}(r,\tau,z|z_s) + (1/r)G_{rzmm}(r,\tau,z|z_s)] \quad ,
\end{aligned} \tag{A-3}$$

and the Green's tensor components are obtained by a temporal integration of the equations

$$\partial_\tau^2 G_{rrmm}(r,\tau,z|z_s) = \lambda(r,z)[\partial_r A_{rmm}(r,\tau,z|z_s) + \partial_z A_{zmm}(r,\tau,z|z_s)$$

$$\partial_\tau^2 G_{\theta\theta mm}(r,\tau,z|z_s) = \lambda(r,z)[\partial_r A_{rmm}(r,\tau,z|z_s) + \partial_z A_{zmm}(r,\tau,z|z_s) + (1/r)A_{rmm}(r,\tau,z|z_s)] + 2\mu(r,z)(1/r)A_{rmm}(r,\tau,z|z_s) + 3M(z_s)(1/2\pi r)\tilde{\delta}(r)\tilde{\delta}(z-z_s)\tilde{\delta}(\tau) \quad ,$$

$$\partial_\tau^2 G_{zzmm}(r,\tau,z|z_s) = \lambda(r,z)[\partial_r A_{rmm}(r,\tau,z|z_s) + \partial_z A_{zmm}(r,\tau,z|z_s) + (1/r)A_{rmm}(r,\tau,z|z_s)] + 2\mu(r,z)\partial_z A_{zmm}(r,\tau,z|z_s) + 3M(z_s)(1/2\pi r)\tilde{\delta}(r)\tilde{\delta}(z-z_s)\tilde{\delta}(\tau) \quad ,$$

$$\partial_\tau^2 G_{rzmm}(r,\tau,z|z_s) = \mu(r,z)[\partial_z A_{rmm}(r,\tau,z|z_s) + \partial_r A_{zmm}(r,\tau,z|z_s)] \quad , \qquad \text{(A-4)}$$

where the bulk modulus $M(z_s)$ in general is

$$M(z_s) = \lambda(z_s) + (2/3)\mu(z_s) \quad , \qquad \text{(A-5)}$$

with $\mu(z_s)$ equal to zero if the source is located in the water layer. No summation over repeated indices r and z are intended in equation (A-3) and equation (A-4). The numerical implementation is performed on a staggered grid, using high-order derivative operators (Holberg, 1987). The time integration is performed to second order. Several implementations of the temporal delta function $\delta(t-t')$ were tested. A pure spike with amplitude $1/\Delta t$ at time t' gave artifacts. Starting from the delta-function definition,

$$\delta(t-t') = (1/\sqrt{\pi})\lim_{\epsilon\to 0}(1/\sqrt{\epsilon})e^{(t-t')^2/\epsilon} \quad , \qquad \text{(A-6)}$$

gave a smoother and much better solution. The parameter ϵ was chosen so small that $\delta(t-t')$ represented a signal with a very high frequency content, but still within the frequency range which could be solved by the high-order finite-difference scheme.

With the Green's tensor known, equation (6) can be used to calculate the pressure response from the overburden at $\mathbf{x}_r$ given a source signature S(t),

$$P_a(\mathbf{x}_r,t) = -(1/9)\int_0^{t^+} dt' \int d^3x' G_{iinn}(\mathbf{x}_r,t-t'|\mathbf{x}',0)\delta(\mathbf{x}'-\mathbf{x}_s)S(t') \quad . \qquad \text{(A-7)}$$

The Green's tensor also gives the stress components at $\mathbf{x}_c$,

$$\sigma_{ij}(\mathbf{x}_c,t) = (1/3)\int_0^{t^+} dt' \int d^3x' G_{ijnn}(\mathbf{x}_c,t-t'|\mathbf{x}',0)\delta(\mathbf{x}'-\mathbf{x}_s)S(t') \quad . \qquad \text{(A-8)}$$

acceleration components a_r^d and a_z^d can be calculated from the equation of motion.

However, the downgoing field at $\mathbf{x}_c$ is needed on a surface and in Cartesian coordinates. The symmetry properties of the downgoing field is used to obtain the complete boundary condition for the 3D simulation in the target volume,

$$\begin{aligned} a_x^d(\mathbf{x}_c) &= a_x^d(x_c,y_c,z_c) = a_r^d(r_c,z_c)\cos(\theta) \quad , \\ a_y^d(\mathbf{x}_c) &= a_y^d(x_c,y_c,z_c) = a_r^d(r_c,z_c)\sin(\theta) \quad , \\ t_x^d(\mathbf{x}_c) &= t_x^d(x_c,y_c,z_c) = t_r^d(r_c,z_c)\cos(\theta) \quad , \\ t_y^d(\mathbf{x}_c) &= t_y^d(x_c,y_c,z_c) = t_r^d(r_c,z_c)\sin(\theta) \quad , \end{aligned} \tag{A-9}$$

where

$$\begin{aligned} r_c &= \sqrt{(x_c^2 + y_c^2)} \quad , \\ \cos(\theta) &= x_c/r_c \quad , \\ \sin(\theta) &= y_c/r_c \quad . \end{aligned} \tag{A-10}$$

APPENDIX B

3D elastic finite-difference modeling of target volume response

The set of coupled partial differential equations for 3D elastic wave propagation are given in Mittet et al. (1988). The medium parameters are staggered as discussed in Mittet and Renlie (1996). The implementation of the boundary condition is reported in Mittet (1994). Let all indices run over their Cartesian values x, y and z and use the Einstein summation convention. Equation (2) is solved by first finding the auxiliary field A_{qmn},

$$A_{qmn}(\mathbf{x},t-t'\,|\,\mathbf{x}',0) = \rho^{-1}(\mathbf{x})\partial_k G_{qkmn}(\mathbf{x},t-t'\,|\,\mathbf{x}',0) \quad . \tag{B-1}$$

The components of the elastic Greens tensor G_{ijmn} is then given by temporal integration of the equation,

where the Hooke's tensor is

$$c_{ijmn}(\mathbf{x}) = \lambda(\mathbf{x})\delta_{ij}\delta_{mn} + \mu(\delta_{im}(\mathbf{x})\delta_{jn} + \delta_{in}\delta_{jm}) \quad . \tag{B-3}$$

The numerical implementation is, as for the cylindrical-symmetric scheme, performed on a staggered grid, using high order derivative operators. The time integration is performed to second order.

With the Green's tensor known, equation (7) can be used to calculate the upgoing response from the target volume at $\mathbf{x}_c'$ given the downgoing field at $\mathbf{x}_c$ as boundary condition,

$$\sigma_{ij}^u(\mathbf{x}_c',t) = \int_0^{t^+} dt' \int d^3x' G_{ijmn}(\mathbf{x}_c',t-t'|\mathbf{x}',0) B_{mn}^d(\mathbf{x}',t') \quad , \tag{B-4}$$

where the boundary condition $B_{mn}^d(\mathbf{x},t)$ is,

$$B_{mn}^d(\mathbf{x},t) = \int_S dS(\mathbf{x}_c)[\delta(\mathbf{x}-\mathbf{x}_c)n_m a_n^d(\mathbf{x}_c,t) + \partial_m\delta(\mathbf{x}-\mathbf{x}_c)t_n^d(\mathbf{x}_c,t)] \quad . \tag{B-5}$$

With the upgoing stress components known at $\mathbf{x}_c'$, the reduced traction components $t_x^u(\mathbf{x}_c',t)$, $t_y^u(\mathbf{x}_c',t)$ and $t_z^u(\mathbf{x}_c',t)$ can be calculated from equation (5) and the upgoing acceleration components $a_x^u(\mathbf{x}_c',t)$, $a_y^u(\mathbf{x}_c',t)$ and $a_z^u(\mathbf{x}_c',t)$ can be calculated from the equation of motion.

APPENDIX C

Cylinder symmetric elastic finite-difference modeling of upgoing field

If the receivers are assumed to be in the water layer, then it is sufficient to calculate $G_{mmij}(\mathbf{x}_r,t|\mathbf{x}_c',t')$ in the overburden to obtain the field at the receivers given the boundary condition for the upgoing field at $\mathbf{x}_c'$. Using spatial reciprocity give,

$$G_{mmij}(\mathbf{x}_r,t|\mathbf{x}_c',t') = G_{ijmm}(\mathbf{x}_c',t|\mathbf{x}_r,t') \quad , \tag{C-1}$$

which implies that the same numerical scheme can be used to calculate $G_{ijmm}(\mathbf{x}_c',t|\mathbf{x}_r,t')$ as was used to calculate $G_{ijmm}(\mathbf{x}_c,t|\mathbf{x}_s,t')$, since there is a spatial translation invariance in the plane-layered overburden. The coordinate $\mathbf{x}_c$ can be

The pressure response at the receivers due to the part of the field interacting with the target volume is given by equation (7),

$$P_b(\mathbf{x}_r,t) = -(1/3)\int_0^{t^+} dt' \int d^3x' G_{mmij}(\mathbf{x}_r,t-t'\,|\,\mathbf{x}',0)B^u_{ij}(\mathbf{x}',t') \quad , \qquad \text{(C-2)}$$

where the boundary condition $B^u_{ij}(\mathbf{x},t)$ is

$$B^u_{ij}(\mathbf{x},t) = \int_S dS(\mathbf{x}'_c)[\delta(\mathbf{x}-\mathbf{x}'_c)n_i a^u_j(\mathbf{x}'_c,t) + \partial_i\delta(\mathbf{x}-\mathbf{x}'_c)t^u_j(\mathbf{x}'_c,t)] \quad . \qquad \text{(C-3)}$$

Here the boundary condition is given by the 3D finite-difference modeling and the Green's tensor by a cylindrical-symmetric finite-difference modeling and an expansion to Cartesian coordinates using the symmetry properties of the Green's tensor in the overburden.